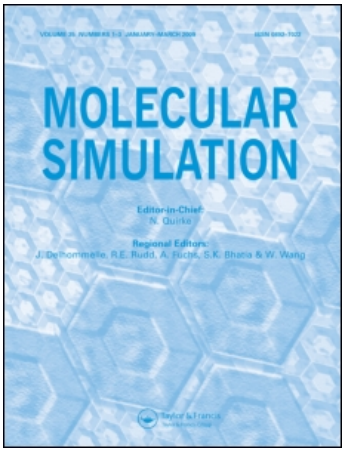

Molecular Simulation
Publication details, including instructions for authors and subscription information:
http://www.informaworld.com/smpp/title~content=t713644482

Propagation speed of a chemical wave front: effect of confinement

J. S. Hansen[a]; B. D. Todd[a]
[a] Centre for Molecular Simulation, Swinburne University of Technology, Melbourne, Australia

First published on: 21 September 2010

To cite this Article Hansen, J. S. and Todd, B. D.(2009) 'Propagation speed of a chemical wave front: effect of confinement', Molecular Simulation, 35: 1, 186 — 192, First published on: 21 September 2010 (iFirst)
To link to this Article: DOI: 10.1080/08927020802235722
URL: http://dx.doi.org/10.1080/08927020802235722

Molecular Simulation
Vol. 35, Nos. 1–2, January–February 2009, 186–192

Taylor & Francis
Taylor & Francis Group

Propagation speed of a chemical wave front: effect of confinement

J.S. Hansen* and B.D. Todd

Centre for Molecular Simulation, Swinburne University of Technology, Melbourne, Australia

(*Received 17 April 2008; final version received 29 May 2008*)

In this paper we perform molecular dynamics simulations of a propagating chemical wave front in both confining and unconfining geometries. It is found that the wave front propagation speed is reduced in the case where the fluid is confined and the channel width is sufficiently small, namely, in the order of 40 molecular diameters. For channel widths larger than 40 molecular diameters the effect from the wall on the front speed is negligible. In the wall–fluid boundary region the self-diffusion is a tensorial property; however, in the channel interior the diffusion is a simple scalar coefficient and equals that of the bulk phase. This fact is used to derive an anisotropic reaction diffusion equation. Via numerical analysis of the reaction diffusion equation it is found that a sufficient condition for the observed speed reduction is that the diffusion element parallel to the wall decreases as the distance to the wall decreases, i.e. in the wall–fluid boundary region. Furthermore, it is found that the front speed is independent of the fluid layering in this region and the normal diffusion element as long as it is non-zero and positive.

Keywords: nanofluidics; confinement; chemical wave front; front speed

1. Introduction

The chemical and physical properties of highly confined fluids have attracted a lot of attention over recent years as a natural part of the development of micro and nano scale devices [26]. On small length scales the classical bulk continuum description may not be adequate. For example, the local transport properties are not equal to those of the corresponding bulk phase and it has been shown that the local (or effective) viscosity may vary appreciatively over several molecular diameters away from the confining wall [13,27]. Furthermore, the transport coefficients should be thought of as non-local properties of the fluid [2,6,12]. These important differences have led to new branches in science that bridge the gab between microscopics and the classical continuum description, namely, microfluidics and nanofluidics [8].

Nano and micro scale devices have a great potential in miniaturisation of chemical processes [26], however, due to the particular properties of highly confined systems thorough studies still need to be carried out in order to fully understand the underlying physico-chemical mechanisms of such devices. In this paper we study a chemical wave front propagating through a slit pore with width ranging from 10 to 50 molecular diameters. The chemical reaction model is the autocatalytic Fisher–Kolmogorov–Petrovsky–Piskunov (FKPP) reaction [10,17]:

$$\mathrm{A} + \mathrm{B} \xrightarrow{k} 2\mathrm{A}. \tag{1}$$

Here A and B are the reactive chemical compounds and k is the rate constant. Consider the simple case where the bulk self-diffusivity of A and B are the same and equal to D, and the initial condition is such that A and B form a sufficiently sharp interface. It can then be shown that the corresponding reaction diffusion equation has a travelling wave front solution with speed [23,30]:

$$c_{\min} = 2\sqrt{kD} \tag{2}$$

where $c_{\min}$ is the minimum speed of all allowed speeds. The FKPP reaction is the prototype of a front propagating into an unstable stationary state and has been studied intensively over the years. For example, Lemarchand et al. [20] have studied the reaction on a mesoscopic level using the Langevin equation and Master equation [19], Brunet and Derrida [5] have investigated the effect of particle discretisation (cut-off effects) on the front speed, Hansen et al. [14] have performed molecular dynamics (MD) simulations to study the effect of the density and size of the reaction zone, and more recently Leda et al. [18] have studied propagation speeds in the non-isothermal situation. Also, Saarloos [31] has made an extensive review which includes very many studies on this system. Despite the extensive literature, no one has to our knowledge studied the FKPP reaction in highly confined systems, and in this paper we study this significant problem, allowing ourselves to focus on the front propagation speed only. We will approach the problem by performing a series of MD simulations of the reaction mechanism, and discuss the results using a local continuum approach.

The paper is organised as follows. In the next section we present how we perform the MD simulations of the

*Corresponding author. Email: jhansen@ict.swin.edu.au

ISSN 0892-7022 print/ISSN 1029-0435 online

DOI: 10.1080/08927020802235722
http://www.informaworld.com

FKPP reaction mechanism in both confining and unconfining geometries. In this section we also present the results from the simulations. In Section 3 we then discuss the MD results in context of a local anisotropic reaction diffusion equation in order to qualitatively understand the underlying mechanism for the observed behaviour. The last section is devoted to conclusions and a few perspective remarks.

2. Molecular dynamics simulations

2.1 Method

When performing MD simulations of propagating chemical wave fronts two problems are imminent: (i) the front speed converges very slowly, thus, very long simulation times are required and (ii) the front characteristics, such as the front width and speed, are greatly affected by the boundaries, hence, very large systems must be simulated. These problems could leave the MD method completely intractable, but can be overcome by applying the periodically expanded molecular dynamics (PEMD) simulation technique introduced by Gorecki [11]. In this method, one master simulation box with dimensions (L_x, L_y, L_z) and periodic boundary conditions is simulated using the standard molecular dynamics technique [1]. We shall denote the position of molecule i in the master box as $\mathbf{r}_i = (x_i, y_i, z_i)$. The actual system is then composed of a number of slave boxes positioned side by side in the front propagation direction, which is here chosen as the x-direction. The mechanical properties of each slave box is simply a replica of the master box, except that the position of molecule i is shifted in the x-direction, such that in slave box n molecule i has the position vector $\mathbf{r}_i = (nL_x + x_i, y_i, z_i)$, $n = 1, 2, 3, \ldots, N_{\text{slaves}} - 1$, where N_{slaves} is the number of slave boxes. We shall throughout this paper use $N_{\text{slaves}} = 100$. Each slave box has its own chemical composition of A and B molecules. The periodic boundaries are of course also applied to the slave boxes. If a molecule crosses a boundary in the x-direction the procedure is accompanied by a change in chemical nature in each slave box when the leaving and entering molecule have different chemical identities. Thus, for example, if molecule i crosses the lower boundary in the x-direction and has identity A in slave box n but B in slave box $n + 1$, the entering molecule in n will be relabelled B. In the last slave box the entering molecule will always be a B molecule, and likewise if the molecule crosses the upper boundary in the x-direction the entering molecule in the first slave box will always be an A molecule. Figure 1 schematically illustrates the PEMD technique in the case where there is no wall present in the system.

The molecules are thought of as simple spherical particles that interact via the truncated and shifted

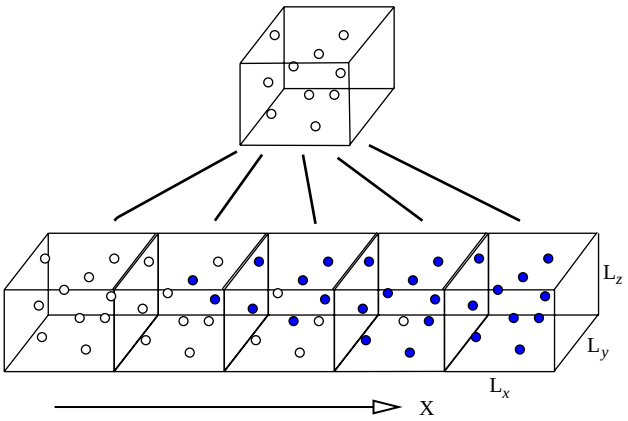

Figure 1. Schematic illustration of the PEMD technique in the unconfined situation, i.e. with no wall present. L_x, L_y and L_z are the dimensions of the master box, and therefore of each slave box. The white particles in the slave boxes are A particles and the black (blue on-line) particles are B particles.

Lennard-Jones potential [1,21]:

$$U_{\text{LJ}}(r_{ij}) = \begin{cases} 4\epsilon\left[\left(\frac{\sigma}{r_{ij}}\right)^{12} - \left(\frac{\sigma}{r_{ij}}\right)^{6}\right] - U_{\text{LJ}}(2.5\sigma) & \text{if } r_{ij} \leq 2.5\sigma \\ 0 & \text{otherwise} \end{cases} \tag{3}$$

where r_{ij} is the distance between particles i and j, and ϵ and σ are the interaction strength and the length scale, respectively. One can express any physical quantity in units of σ, ϵ and mass m. Thus, the temperature, T, can be expressed in dimensionless (or reduced) units as $T* = k_{\text{B}}T/\epsilon$, number density as $\rho* = \rho\sigma^3$, time as $t* = t/(\sigma\sqrt{m/\epsilon})$ and so forth. Here k_{B} is the Boltzmann constant and the number density is defined as the number of particles per unit volume. We will, as is common practice, for the remainder of the paper express all quantities in reduced units and drop the asterisk altogether. All particles are physically identical in the sense that they interact through the same interaction potential independent of their chemical identity. Initially, all particles in the master box are arranged on a body centred cubic lattice with number density $\rho = 0.86$ such that $(L_x, L_y, L_z) = (8.4125, L_y, 8.4125)$. In the case of a confined fluid, the first three layers of particles in the y-direction are label W (wall particles), hence, the wall density is $\rho_{\text{W}} = 0.86$. These choices of number of wall layers and wall density ensure that the fluid particles cannot penetrate or interact across the wall boundary. In this way the confined geometry will resemble a slit pore and in this situation L_y will denote the channel width and not the simulation box width. The wall particles interact with A, B as well as other wall particles via the Lennard-Jones potential given in Equation (3). In each simulation

Table 1. Parameter values used in this paper, the resulting self-diffusion coefficient, reaction rate constant and front speed.

T	ρ_W	ρ	s_f	L_x, L_z	r_{cr}	D	k (10^{-2})	c_{min}
1.5	0.86	0.6	0.005	8.1425	0.98	0.238	1.88	0.134

The self-diffusion coefficient and rate constant are from [14].

run the fluid number density is set to $\rho = 0.6$ for both the confined and unconfined situation by simply removing the correct number of fluid particles in the system. All particle positions are copied to the slave boxes, and all particles in the first 50 slave boxes are labelled A and the particles in the last 50 slave boxes are labelled B. This ensures a sufficiently steep initial concentration profile. The particles in the master box are coupled to a Nose–Hoover thermostat [16,24], such that the temperature is $T = 1.5$, and the equation of motion is then integrated forward using a leap-frog algorithm [1] using a time step of $h = 0.005$. It should be mentioned that we apply a homogeneous thermostat which ensures an average temperature of $T = 1.5$, however, in the region adjacent to the wall the local fluid temperature may vary due to the density variations, hence, an inhomogeneous thermostat should in principle be applied [3]. We will, nevertheless, here ignore these possible small variations. In the presence of a wall, the wall particles, W, are kept fixed around their lattice positions via a restoring spring potential [29]:

$$U_s(\mathbf{r}_i) = \frac{1}{2} k_s (\mathbf{r}_l - \mathbf{r}_i)^2 \tag{4}$$

where $\mathbf{r}_l$ is the lattice site and k_s is the spring constant and is set to $k_s = 100$, which together with the density of $\rho_W = 0.86$ ensure a relatively rigid impenetrable wall with sufficient thermostating properties.

Whenever two fluid particles in the master box are sufficiently close together, i.e. if $r_{ij} < r_{cr}$ where r_{cr} is some number, the corresponding particles in the slave boxes may react according to Equation (1). This is done simply by changing the B particle's label to A. The critical reaction distance, r_{cr}, must be sufficiently small, such that the reacting particles need to possess sufficient kinetic energy to overcome a repulsive part of the Lennard-Jones potential which defines a reaction activation energy [15]. We shall use the value $r_{cr} = 0.98$ as in [14]. Not all particles will react even though they possess enough kinetic energy due to steric effects [25]. To this end, we set a steric factor, s_f, to 0.005 such that if a random number picked out from a uniform distribution in the interval [0;1] is smaller than s_f then the reaction occurs. This value of s_f ensures that the speed distribution of both reactants and products are Maxwell–Boltzmann distributed. We shall use these particular values of s_f, r_{cr}, ρ and T since it enables a direct comparison with previous work [14].

The front position is here defined to be where the density of A is equal to that of B, i.e. $\rho_A = \rho_B$. As the reactions proceed the chemical front will propagate in the x-direction towards high concentration of B. For every ten time steps it is determined how far the front has progressed and the particles are all translated such that the front is positioned at $L_x N_{slaves}/2$. Every time this translation is performed the relevant chemical identities are changed of the particles that cross the x boundaries as described above. The translation determines the front speed, c, and allows the system to be simulated indefinitely, i.e. it basically transforms the system into a moving frame keeping the front position fixed at $z = 0$ where $z = x - ct$ is the front position in the moving frame. It should be mentioned that for unconfined systems where the volume can be determined exactly the front speed can be calculated directly by counting the number of reactions, which reduce data noise considerably [14]. However, for confined systems the fluid volume is ambiguously defined and not exact, leaving that method inadequate.

For a reactive unconfined Lennard-Jones fluid at the state point $(T,\rho) = (1.5,0.6)$, for $s_f = 0.005$ and $r_{cr} = 0.98$, the self-diffusion coefficient is found to be $D = 0.238$ and the reaction rate constant is 0.0188 [14]. This means that $c_{min} = 0.134$ according to Equation (2). This value alongside D, k and all the MD parameters used here are listed in Table 1.

2.2 Results

In Figure 2 the running sample mean of the front speed is depicted as a function of time for a confined fluid with a channel width $L_y = 10.01$. As mentioned earlier, L_y is the channel width in the confined case, where the fluid density

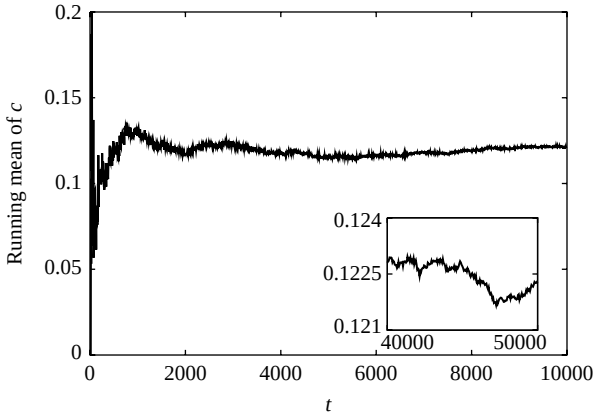

Figure 2. An example of the running sample mean of the front speed, c, as a function of time, t. The system is confined with $L_y = 10.01$. The inset shows the fluctuations around the overall mean (0.122) in the last 2 million time steps.

is non-zero. Figure 3 shows the front propagation speed as a function of L_y in both the confined and unconfined situations. From this figure it is seen that the front speed has a lower value for the confined system and for relatively small channel widths. The difference in front speeds decreases as the channel width increases, indicating that the wall effects become negligible for sufficiently large L_y. Another important point is that the front speed increases for increasing L_y in both situations. That is, the speed depends on the size of the reaction zone. Recall from Table 1 that the classical prediction leads to $c_{\min} = 0.134$. This has been reported earlier [14] and is connected to the fact that in real systems one is dealing with discrete numbers of particles which introduces a cut-off factor in the reaction diffusion equation [5,14]. (Moro [22] also expresses this effect via a correlation volume.) We shall not discuss this point further in this paper, since we only wish to study the effect of the confinement.

In order to investigate the mechanisms behind the reduced front speed, the density profile normalised with respect to the bulk density ($\rho = 0.6$) is plotted in Figure 4 near the wall for a confined system. As it has been shown previously in numerous works (see for example [28]), a layering of the fluid near the wall is observed. This layering has two effects. First, in the region adjacent to the wall the fluid has a crystal-like structure, which will result in very low molecular diffusivity. Secondly, in the wall–fluid boundary region the fluid is anisotropic. Thus, near the wall the self-diffusion is a tensoral property and must be characterised via the second rank diffusion tensor, $\mathbf{D}$. However, in the interior of the channel the fluid is isotropic and the diagonal elements in the diffusion tensor elements have values that are equal to the self-diffusion coefficient in the bulk phase, D, i.e. the diffusion can be thought of as a simple scalar property. Thus for a confined fluid in our geometry, the diffusion tensor itself is a function of y, and should be written as $\mathbf{D} = \mathbf{D}(y)$. In the moving frame and in the case of the unconfined system the front position is located at $z = 0$ and is independent of the y coordinate. In Figure 4 the front position is also plotted as a function of y in the confined situation. The front position is normalised with respect to $N_{\text{slaves}}L_x$ and shifted by plus one, i.e. the front is positioned at $z + 1$ in order to correlate the front position and the density profile. It is seen that the front position is varying in y and that it indeed correlates with the density variations, such that at points of high density the front is ahead of points with lower density. This is likely due to the fact that in the high density regions the non-linearity in the reaction term leads to very large concentration gradients in the x-direction and therefore large fluxes of A.

3. Discussion

We will here base our discussion of the molecular dynamics results on the corresponding phenomenological continuum description. This means that we shall limit ourselves to understand the main underlying mechanisms for the observed speed reduction, since, for example, the continuum description fails to capture the effect of the Brunet cut-off factor as mentioned earlier and we can therefore not expect any quantitative agreement with the MD results. The balance equation for the chemical compound A can be written as [7]:

$$\frac{\partial \rho_{\text{A}}}{\partial t} = f(\rho_{\text{A}}) - \nabla \cdot \mathbf{J}_{\text{A}} \tag{5}$$

where $f(\rho_{\text{A}})$ is the mass production of A per unit volume per unit time and $\mathbf{J}_{\text{A}}$ is the mass flux vector of chemical A. The flux can be related to the density gradient via Fick's law [7]:

$$\mathbf{J}_{\text{A}} = -\mathbf{D}(y) \cdot \nabla \rho_{\text{A}} \tag{6}$$

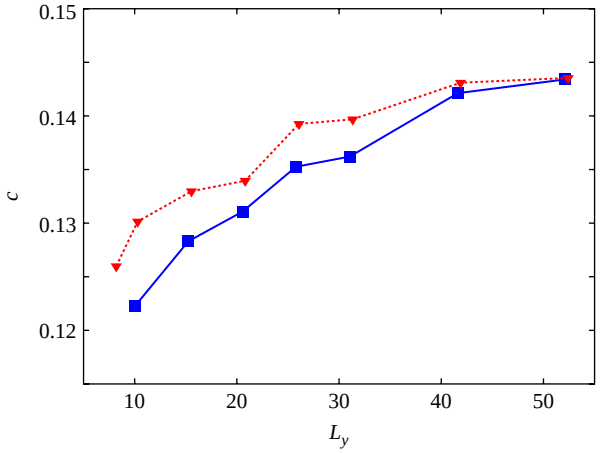

Figure 3. Front propagation speed as a function of L_y for the confined situation (filled squares connected with full lines) and the unconfined situation (triangles connected with punctured lines). The lines serve as a guide to the eye.

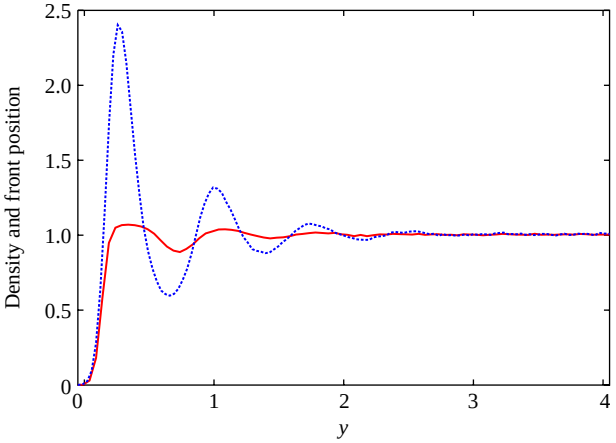

Figure 4. Punctured line: Density profile normalised with the bulk density ($\rho = 0.6$) near the wall. Full line: Front position in the moving frame ($z + 1$) as a function of y.

where we have explicitly shown the diffusion tensor's y dependence as discussed above in Section 2.2. If we assume the off diagonal elements are zero, i.e. gradients in one direction do not lead to a flux in other directions, $\mathbf{D}(y)$ is [4]:

$$\mathbf{D}(y) = \begin{bmatrix} D_{\parallel}(y) & 0 & 0 \\ 0 & D_{\perp}(y) & 0 \\ 0 & 0 & D_{\parallel}(y) \end{bmatrix} \tag{7}$$

where $D_{\parallel}(y)$ and $D_{\perp}(y)$ are the diffusion elements parallel and normal to the wall, respectively. According to reaction kinetics [25] the reaction term can be written as:

$$f(\rho_A) = k\rho_A(\rho(y) - \rho_A) \tag{8}$$

where $\rho(y)$ is the total local density of the fluid which varies close the wall according to Figure 4. Substituting Equations (6)–(8) into Equation (5) and ignoring concentration gradients in the z-direction the anisotropic reaction diffusion equation reads:

$$\frac{\partial \rho_A}{\partial t} = k\rho_A(\rho(y) - \rho_A) + D_{\parallel}(y)\frac{\partial^2 \rho_A}{\partial x^2} + \frac{\partial}{\partial y}D_{\perp}(y)\frac{\partial \rho_A}{\partial y}. \tag{9}$$

The mixed boundary conditions are:

$$\left.\frac{\partial \rho_A(x,y,t)}{\partial y}\right|_{y=0} = \left.\frac{\partial \rho_A(x,y,t)}{\partial y}\right|_{y=L_y} = 0$$

$$\text{and } \rho_A(-\infty, y, t) = \rho(y), \ \ \rho_A(\infty, y, t) = 0. \tag{10}$$

Equation (9) together with the boundary conditions in Equation (10) is solved numerically using different functional forms for $\rho(y)$ setting $D_{\perp}(y) = D_{\parallel}(y) = 1$. We have here applied a simple first order scheme with respect to time and a second order central difference scheme with respect to the spatial coordinates [9]. An example is shown in Figure 5 where the front position and the density are plotted as functions of y. It can be seen that the front position varies in a damped oscillatory manner which correlates with the density variation. This was also observed in the MD simulations. The variation in density will, however, not decrease the front speed. In fact, this is also observed for different functional forms of the normal diffusion element $D_{\perp}(y)$. From the numerical analysis it is found that a sufficient condition for a decrease in the front speed is:

$$\frac{D_{\parallel}(y)}{dy} > 0 \ \text{ in the boundary region.} \tag{11}$$

As discussed in Section 2.2, the local diffusivity near the wall is very small and increases to that of the bulk diffusivity in the channel interior, which is consistent with

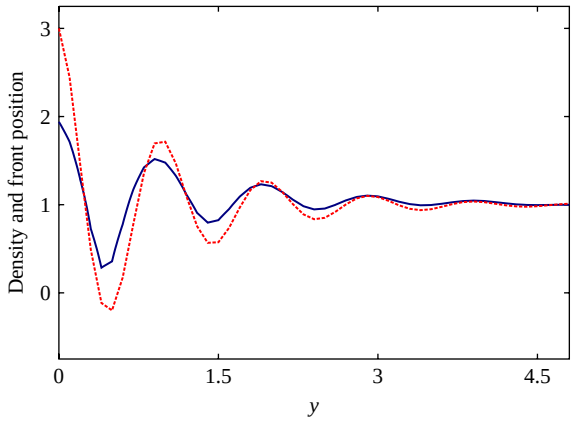

Figure 5. Full line: Snap shot of the front position as a function of y. Punctured line: Density profile as a function of y : $\rho(y) = 1 + e^{-y}\cos(\pi y)$. The quantities are scaled and shifted for comparison and are given in arbitrary units.

Equation (11). This suggests a simple functional form for the parallel diffusion element:

$$D_{\parallel}(y) = D(1 - e^{-\alpha y}) \tag{12}$$

where α is a scalar that determines the convergence to the bulk diffusivity, D. Thus, setting $\rho(y) = \rho$, $D_{\perp}(y) = D$ and using Equation (12) we obtain a simplified reaction diffusion equation:

$$\frac{\partial \rho_A}{\partial t} = k\rho_A(\rho - \rho_A) + D\left[(1 - e^{-\alpha y})\frac{\partial^2 \rho_A}{\partial x^2} + \frac{\partial^2 \rho_A}{\partial y^2}\right] \tag{13}$$

In Figure 6 the relative front speed difference with respect to $c_{\min}$ is plotted as a function of L_y, where $\alpha = D = k = \rho = 1$ in which case $c_{\min} = 2.0$ according to Equation (2). It can be seen that the front speed, c, converges to $c_{\min}$ for high values of L_y which corresponds to the situation depicted in Figure 3. This indicates that the underlying mechanism for the observed reduction in front speed is linked to a reduced diffusion parallel to the wall in the wall–fluid boundary region.

It would be of great value to show analytically that the front speed is reduced for confined systems. To this end one could simplify the problem by studying the reaction diffusion equation, Equation (13), at the wall–fluid boundary $y = 0$ and in the front edge [23,31] where $D(1 - e^{-\alpha y}) \approx Dy$ and $\rho_A(\rho - \rho_A) \approx \rho\rho_A$. It can then easily be shown that the corresponding travelling wave equation can be written as:

$$D\left[y\frac{\partial^2 u}{\partial z^2} + \frac{\partial^2 u}{\partial y^2}\right] + c\frac{\partial u}{\partial z} + k\rho u = 0 \tag{14}$$

where $u(z, y) = \rho_A(x, y, t)$. The linear partial differential equation with a variable coefficient is not readily solved by standard means, since it, for example, does not allow for separation of variables, standard pertubation methods,

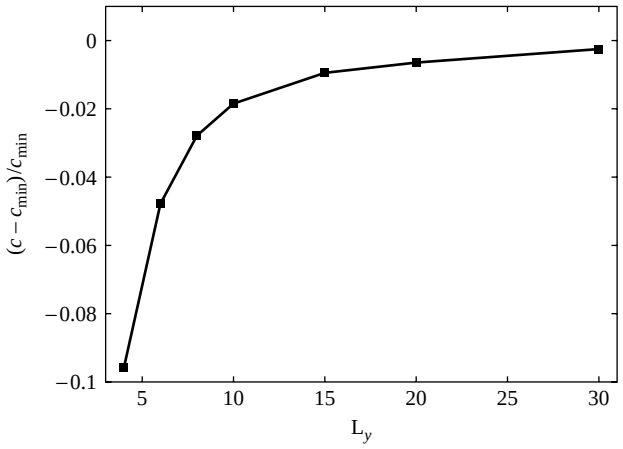

Figure 6. Relative front speed difference between c and c_{min} as a function of channel width L_y where $\alpha = D = k = \rho = 1$ and $c_{min} = 2$. Line serves as a guide to the eye.

or tractable Fourier transforms. To complicate things further, at the wall–fluid boundary, $y = 0$, Equation (14) is parabolic whereas away from the wall, $y > 0$, it is elliptic. This means that the standard analytical approach is basically not feasible, which is the reason why we have applied the numerical analysis rather than a rigorous analytical solution to the problem.

4. Conclusion

In this paper we have performed MD simulations of a propagating chemical wave front in confining and unconfining geometries. We find from the MD simulations that the front propagation speed is reduced in the case where the fluid is confined and the channel width is sufficiently small, namely of the order of 40 molecular diameters. For channel widths larger than 40 molecular diameters the effect from the wall on the front speed is negligible. Near the wall–fluid boundary the fluid has a crystal-like structure in the direction normal to the wall. This means that the diffusion is a tensorial property in this region. However, in the channel interior the diffusion is a simple scalar property and equals that of the bulk phase. We have used this information to derive an anisotropic reaction diffusion equation, Equation (9). Via numerical analysis we have found that a sufficient condition for the observed speed reduction is that the diffusion element parallel to the wall decreases in the wall–fluid boundary region. Furthermore, the numerical study indicates that the final front speed is independent of the fluid layering in this region and the normal diffusion element as long as the normal diffusivity is non-zero and positive.

In this paper we have made a first analysis of a chemical wave front's propagation speed in a confining geometry. The analysis should be extended in the future. For example, the diffusivity is a non-local property of the fluid at the nanoscale [2,6,12] and not a local property as assumed here. We have also assumed that the diffusion tensor is a diagonal tensor; however, this might not be true in general, leading to cross coupling terms which could have an effect on the mass diffusivity, the rate constant itself dependents on the local density [25], etc. These effects may influence the front propagation speed, and it would be useful to estimate their individual importance. Another important point to mention is that the front propagation speed depends on the number of particles in the reaction zone. If a thorough quantitative analysis is to be carried out, this effect must indeed be correctly modelled and included.

References

[1] M.P. Allen and D.J. Tildesley, *Computer Simulation of Liquids*, Clarendon Press, New York, 1989.
[2] W.E. Alley and B.J. Alder, *Generalized transport coefficients for hard spheres*, Phys. Rev. A 271 (1983), pp. 3158–3173.
[3] A. Baranya, D.J. Evans, and P.J. Daivis, *Isothermal shear-induced heat-flow*, Phys. Rev. A 46 (1992), pp. 7593–7600.
[4] H. Bock, K.E. Gubbins, and M. Shoen, *Anisotropic self-diffusion in nanofluidic structures*, J. Phys. Chem. C 111 (2007), pp. 15493–15504.
[5] E. Brunet and B. Derrida, *Shift in the velocity of a front due to a cutoff*, Phys. Rev. E 56 (1997), pp. 2597–2604.
[6] P.J. Cadusch, B.D. Todd, J. Zhang, and P.J. Daivis, *A non-local hydrodynamic model for the shear viscosity of confined fluids: Analysis of homogeneous kernel*, J. Phys. A 41 (2008), 035501.
[7] S.R. de Groot and P. Mazur, *Non-Equilibrium Thermodynamics*, Dover Publications, New York, 1984.
[8] J.C. T. Eijkel and A. van den Berg, *Nanofluidics: What is it and what can we expect from it?* Microfluidics Nanofluidics 1 (2005), pp. 249–267.
[9] J.H. Ferziger and M. Perić, *Computational Methods for Fluid Dynamics*, Springer-Verlag, New York, 2002.
[10] R.A. Fisher, *The wave of advance of advantageous genes*, Ann. Eugenics 7 (1937), pp. 335–369.
[11] J. Gorecki, *Molecular dynamics simulations of a chemical wave front*, Physica D 84 (1995), pp. 171–179.
[12] J.S. Hansen, P.J. Daivis, K.P. Travis, and B.D. Todd, *Parameterization of the nonlocal viscosity kernel for an atomic fluid*, Phys. Rev. E 76 (2007), 041121.
[13] J.S. Hansen, P.J. Daivis, and B.D. Todd, *Local linear viscoelasticity of confined fluids*, J. Chem. Phys. 126 (2007), 144706.
[14] J.S. Hansen, B. Nowakowski, and A. Lemarchand, *Molecular dynamics simulations and master-equation description of a chemical wave front: Effect of density and size of reaction zone on propagation speed*, J. Chem. Phys. 124 (2006), 034503.
[15] J.S. Hansen, S. Toxvaerd, and E.L. Præstgaard, *Propagation of a planar flame front studied by molecular dynamics*, J. Chem. Phys. 31 (2003), pp. 13039–13045.
[16] W.G. Hoover, *Canonical dynamics: Equilibrium phase-space distributions*, Phys. Rev. A 31 (1985), pp. 1695–1697.
[17] A. Kolmogorov, I. Petrovsky, and N. Piskunov, *Study of the diffusion equation with growth of the quantity of matter and its application to a biology problem*, Bull. Univ. Moscow Ser. Int. Sec. A 1 (1937), pp. 1–72.
[18] M. Leda, A. Lemarchand, and B. Nowakowski, *Forbidden interval of propagation speed for exothermic chemical fronts*, Phys. Rev. E 75 (2007), 056304.
[19] A. Lemarchand, *Selection of an attractor in a continuum of stable solutions: Description of a wave front at different scales*, J. Stat. Phys. 101 (2000), pp. 579–598.

[20] A. Lemarchand, A. Lesne, and M. Mareschal, *Langevin approach to a chemical wave front: Selection of the propagating velocity in the presence of internal noise*, Phys. Rev. E 51 (1995), pp. 4457–4465.
[21] D.A. Mcquarrie, *Statistical Mechanics*, Harper and Row, New York, 1976.
[22] E. Moro, *Hybrid method for simulating front propagation in reaction–diffusion systems*, Phys. Rev. E 69 (2004), 060101.
[23] J.D. Murray, *Mathematical Biology*, Springer-Verlag, New York, 1989.
[24] S. Nosé, *A molecular dynamics method for simulation in the canonical ensemble*, Mol. Phys. 52 (1984), pp. 255–268.
[25] J.I. Steinfeld, J.S. Francisco, and W.L. Hase, *Chemical Kinetics and Dynamics*, Prentice Hall, Englewood Cliffs, NJ, 1998.
[26] P. Tabeling, *Introduction to Microfluidics*, Oxford University Press, Oxford, 2005.
[27] B.D. Todd, D.J. Evans, and P.J. Daivis, *Pressure tensor for inhomogenous fluids*, Phys. Rev. E 52 (1995), pp. 1627–1638.
[28] S. Toxvaerd, *The structure and thermodynamics of a solid–fluid interface*, J. Chem. Phys. 74 (1981), pp. 1998–2005.
[29] K.P. Travis, B.D. Todd, and D.J. Evans, *Departure from Navier–Stokes hydrodynamics in confined liquids*, Phys. Rev. E 55 (1981), pp. 4288–4295.
[30] W. van Saarloos, *Dynamical velocity selection: Marginal stability*, Phys. Rev. Lett. 58 (1987), pp. 2571–2574.
[31] W. van Saarloos, *Front propagation into an unstable states*, Phys. Rep. 386 (2003), pp. 29–222.